https://doi.org/10.5194/os-2020-90
Preprint. Discussion started: 17 September 2020

Ocean Science
Discussions
Open Access
EGU

Impact of naval traffic on the sediment transport of the Port of Genoa – a modelling study

Antonio Guarnieri [(1)], Sina Saremi [(2)], Andrea Pedroncini[(3)] Jacob H. Jensen[(2)], Silvia Torretta[(3)] Marco Vaccari[(4)], Caterina Vincenzi [(4)]

(1) Istituto Nazionale di Geofisica e Vulcanologia, Sezione di Bologna, Via D. Creti, 12, 40128 Bologna, Italy

(2) DHI, Horsholm, Denmark

(3) DHI S.r.l., Via Bombrini 11/12, 16149 Genova

(4) Autorità di Sistema Portuale del Mar Ligure Occidentale (Genova), Palazzo San Giorgio - Via della Mercanzia 2

Corresponding author: Antonio Guarnieri; antonio.guarnieri@ingv.it

https://doi.org/10.5194/os-2020-90
Preprint. Discussion started: 17 September 2020

Ocean Science
Discussions
Open Access
EGU

Abstract

The action of propellers induced jets on the seabed of ports can be responsible of erosion and deposition of sediment around the port basin, potentially inducing important variations of the bottom topography in the medium to long time scales. Such dynamics constantly repeated for long periods can result in drastic reduction of ships' clearance - in the case of accretion - or might be a threat for the stability and duration of the structures - in the case of erosion. These sediment related processes are sources of problems for the port managing authorities, both for the safety of navigation and for the optimization of the management and maintenance activities of the ports' bottom and infrastructures.

In the present work we study the erosion and sediment transport induced by the action of the vessel propellers of naval traffic in the passenger Port of Genoa (Italy) by means of integrated numerical modeling and we propose a novel methodology and state of the art modeling science-based tools useful to optimize and efficiently plan the ports managing activities and the of maintenance of ports seabed.

1 - Introduction

Operational activities of harbors and ports are tightly related to the local bathymetry, which must be as deep as to guarantee the regular passage, maneuvering and berthing of ships. On the contrary, ships clearance is often so limited that the safety of in-port navigation might be at risk and ships may even hit the sea bed in extreme cases. This is a source of high criticalities, not only for safety sake, but also for the consequent rise of problems related to an efficient management and maintenance of the bottom and of the port infrastructure in general.

Ships' traffic inside ports is responsible for the generation of intense current jets produced by the action of the main propellers, as sketched in Figure 1. Such velocities induce shear stresses on the sea bottom which can possibly result in sediment resuspension, when exceeding the critical stress for erosion (Van Rijn, 2007, Soulsby et al., 1994, Grant and Madsen, 1979). Before depositing back onto the sea floor, the re-suspended sediment might be widely transported around the basin by the combined effect of natural currents, such as those induced by tides, winds or density gradients, and vessels' related currents, such as those directly induced by propellers or again by the movement and displacement of the ships. Therefore, the continuous traffic in and out ports could result in the displacement of a great amount of seabed material which can, in turn, induce important variations of the bathymetry in the medium to long time scales. The result of these variations is the possible formation of erosional or depositional trends for specific areas of port basins.

https://doi.org/10.5194/os-2020-90
Preprint. Discussion started: 17 September 2020

Ocean Science
Discussions
Open Access
EGU

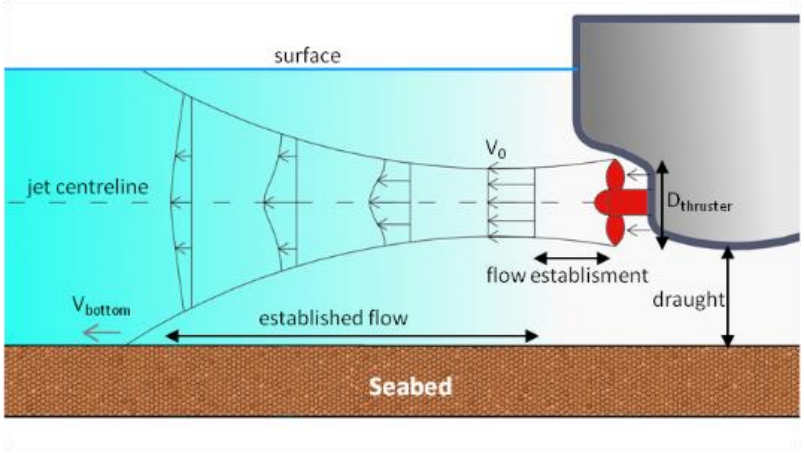

Figure 1 - Example of propeller induced jet of a moving ship (main propulsion without rudder)

These processes can have direct impact on the operability of ports and on safety depths for navigation (Mujal-Colilles et al., 2016, Castells et al., 2018). If such dynamics are particularly relevant and fast (bottom accretion of the order of tens of centimeters per year, or even higher) they induce port authorities to undergo dredging operations for the maintenance of the seabed in order to fully recover the required clearance and operational conditions necessary for undisturbed ships motion, maneuvering and berthing.

The majority of published literature and studies about the effects of ships' propellers on port sediments and structures is experimental., mainly conducted in laboratories with the use of physical models (Castells et al. 2018), while port authorities suffer from the lack of practical instruments available to provide robust and scientifically based studies and predictions of the described processes. Such tools would allow for an aware planning of specific actions aimed at the maintenance of the seabed. This would help to guarantee the continuity in the operational activities of ports on one side, and to the optimization of the involved economic resources on the other side. In fact, the need of unplanned maintenance activities usually implies additional costs due to operating in emergency conditions and in some cases to the partial interruption of the service.

The integrated numerical modeling of hydrodynamics and sediment transport may represent an important aid to Port Authorities and more broadly to port managers and operators. It could be used to reproduce and better understand the seabed sediment dynamics induced by ships' propellers on the short, medium and long-time scales and so provide the needed tools in the perspective of an efficient operational maintenance of the seabed. Such tools can be used in delayed mode in order to reproduce the major sediment processes in the past - as it is the present case - or even in forecast mode through the implementation of real time operational services.

https://doi.org/10.5194/os-2020-90
Preprint. Discussion started: 17 September 2020

So far, the issue of propeller's induced jet has been mainly studied through empirical approaches, usually relying either on the German method (MarCorm WG, 2015, Grabe, et al. 2015, Abromeit et al., 2010,), or on the Dutch method (CIRIA et al., 2007). In such approaches, empirical formulas are introduced in order to estimate the propeller wash on the sea bed in terms of induced velocities and resulting induced shear stresses, depending on specific characteristics of the ships and ports of interest, such as the propeller's typology, diameter, rotation rate and ship's draught. The resulting induced velocities are usually considered only locally for the technical design of mooring structures and for considerations on the protection of port's infrastructures in general. Besides the assumptions introduced in the empirical formulas, such an approach is punctual and does not provide the full picture of the three dimensional evolution of the induced jet throughout the water column at any distance from the propeller, in any location of the port. The tool is therefore not suitable for a comprehensive management of the ports in a broader way.

The present work shows a pilot study of seabed evolution induced by ships' propellers in the passenger area of the Port of Genoa (Figure 2), where the naval traffic involves mainly passenger vessels (ferries and cruise ships, generally self-propelled) and where the resulting sediment dynamics (erosion/deposition rates) is particularly relevant: estimated in the order of several tens of centimeters per year (direct communication from the Port Operators and analysis of bathymetric surveys at different time). The proposed approach is based on fully integrated high resolution numerical modeling of three-dimensional hydrodynamics and sediment transport.

The manuscript is organized as follows: in Sect. 2 we introduce the adopted methodology, while the data available for the study are presented in Sect. 3. Sect. 4 describes the numerical models used. The results of the numerical simulations are presented in Sect. 5 and discussed in Sect. 6, which offers some conclusions as well.

2 – Methods

The study is based on the latest versions of the hydrodynamic and mud transport models MIKE 3 FM (DHI, 2017) which will be described in detail in Sect. 3 and in APPENDICES A1 and A2.

In order to resolve in a realistic way the propellers induced jet, a very high resolution was adopted in the numerical model both in the vertical and in the horizontal: approximately 1-2 meters and 5 meters, respectively. This, together with the use of a non-hydrostatic version of the hydrodynamic model allowed to reproduce very accurately the processes and the main patterns of the current field generated by the ships propellers during the navigation and maneuvering inside the port.

As shown in Figure 2, 12 docks have been included in the study (marked with orange or red lines indicating ferry or cruise vessels, respectively). Only passenger ships were studied. The turning basins where arriving vessels undergo maneuvers for berthing are represented in Figure 2 with the white dashed circles marked as *a* and *b*. Circle *a* refers to

https://doi.org/10.5194/os-2020-90
Preprint. Discussion started: 17 September 2020

vessels berthing at docks T5 to T11, while circle *b* refers to vessels to docks T1 to T3. Finally, the turning area for vessels arriving to docks D.L., 1012 and 1003 is at the entrance of the port and is not simulated in this study since it is out of the area of interest.

The general methodology adopted is organized in different phases, as follows:

1. *Assessment of the naval traffic during a typical year*. This was fundamental to understand the typical dynamics of the naval traffic in the different sectors of the port and to identify the characteristics of the ships that most impact hydrodynamics and sediment re-suspension from the bottom, such as the size of the ships, the related draught, the dimension of the propellers and their typical rotation rates. The results of the analysis, which will be detailed in Sect. 4.1, led also to the definition of one most representative synthetic vessel for each berth of the port.
2. *Implementation of a high-resolution 3D hydrodynamic model of the port of Genoa*. The numerical hydrodynamic model that we implemented took into account the ship routes, both entering and exiting the port, as analyzed within the previous vessel traffic analysis phase. As it will be detailed in Sect. 4.1, 24 different simulations of the hydrodynamic model have been implemented, one for each dock and route considered (docking and undocking). The resulting 24 different scenarios have been simulated separately. This allowed to analyze the effect of each vessel's passage on the induced hydrodynamics in the basin. The single hydrodynamic contributions were then used to drive the sediment transport model. The present approach won't therefore consider potential simultaneous interactions amongst hydrodynamic patterns generated by different propellers, assuming that very close passages of different vessels are unlikely to happen.
3. *Implementation of a coupled sediment transport model*. Based on the available data, a numerical model of sediment resuspension and transport for fine-grained and cohesive material was implemented. The model was coupled to the hydrodynamics resulting from the 24 different vessels scenarios. As with the hydrodynamic component, the simulations of the sediment model were carried out separately.
4. *Gathering of the separate results and overall analysis*. The effects of the passage of the single vessels on the bottom sediment have been summed-up to each other in terms of erosion/deposition according to the overall number of passages over the one-year period of time previously analyzed. This led us to provide information on the resulting annual sediment dynamics.

A semi-quantitative calibration/validation of the modeling results was possible through the comparison of the seabed evolution reproduced with the integrated modeling system and the differential bathymetric maps derived from different surveys of the port topography at approximately one year interval.

https://doi.org/10.5194/os-2020-90
Preprint. Discussion started: 17 September 2020

Ocean Science
Discussions
Open Access
EGU

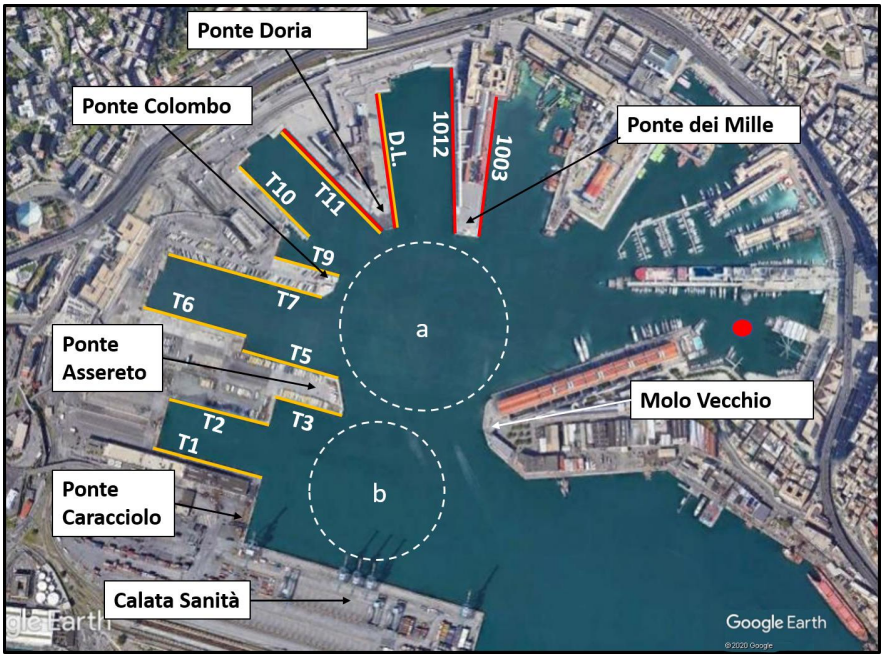

Figure 2 - Passenger port of Genoa. The colored lines along the docks refer to the typology of the operating ships: red lines indicate cruise vessels while orange lines indicate ferries. The names of the docks (in white) are next to the colored lines are. The red dot represents the location of the station where sediment samples with physical information on the grains are available (see Sect. 4.2). The white dashed circles marked as *a* and *b* represent the turning areas for vessels berthing to docks T5 to T11 and to T1 to T3

3 – Available data and information

The most relevant data necessary for the implementation of the work were provided by the Port Authority of Genoa and Stazioni Marittime SpA, which cover the role of Port Authority and main Port Operator in the target area, respectively.

3.1 – Bathymetry

Several bathymetry surveys of the different sectors of the port were available at different resolutions in the domain of interest. The dataset used for the simulations was the result of the merging of the latest available surveys (March-June 2018) in the inner sectors of the port delivered on a regular grid of 5 meters of resolution. Figure 3 shows the latest available observed bathymetry of the entire port (left panel) and a zoom focused on *Ponte Colombo* and the surrounding basin. A few tens of meters off the right edge of *Ponte Colombo* and *Ponte Assereto* (see Figure 2) a deep natural pit in the bathymetry is clearly visible, reaching approximately 22 meters below the water surface. This area has often been

https://doi.org/10.5194/os-2020-90
Preprint. Discussion started: 17 September 2020

used in the past by the Port Authority as a preferred site for dumping the sediment resulting from recurring maintenance dredging operations of the seabed in those sectors where depositional trends are large enough to reduce vessels clearance and to impact on the safety of navigation inside the port. Moreover, the same depressed area is largely used as a turning area by the passenger ferries heading to docks T5, T6, T7 and T9, which cover approximately the 50% of the entire naval traffic of the basin (see Sect. 4.1): during manoeuvres over this pit the turning ferries produce intense turbulence which may reach the newly dumped material resulting from the dredging operations. This material is still rather loose and consequently subject to be easily re-suspended and transported again around the port basin, nullifying the results of the dredging operations.

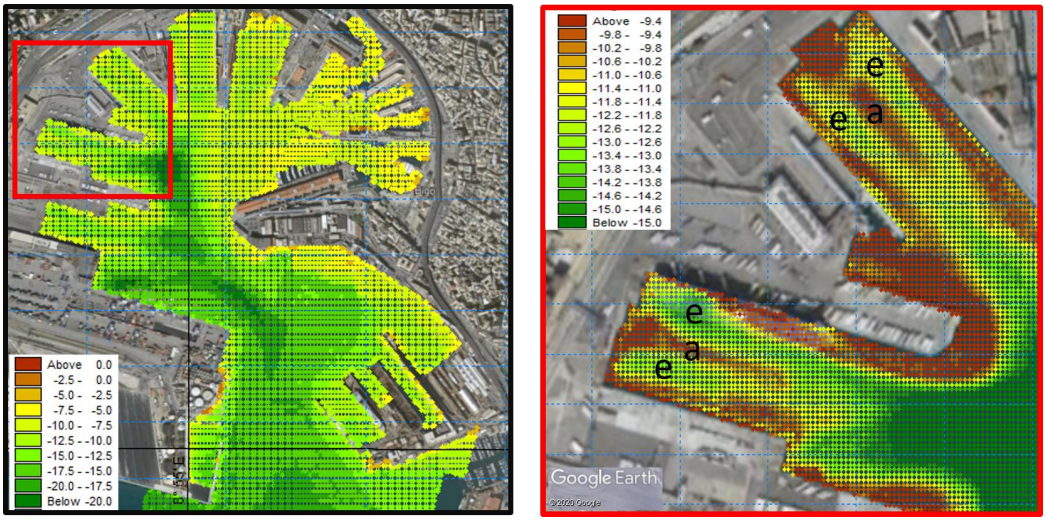

Figure 3 - Bathymetry of the port of Genoa. Entire Passenger Port (left panel) and zoom on *Ponte Colombo* and the surrounding basins (from T5 to T11, right panel)

Additionally, the bathymetry presented in the right panel of Figure 3 shows a pattern of erosion and accumulation common to the majority of the wet basins confined amongst the different docks. Here, the propellers activity when vessels leave or approach the berth induces areas of erosion identified with channels of deepened bathymetry (referred to with an "*e*" in the right panel of Figure 3, where colours are yellow-green) and areas of accumulation identified with tongues of shallower bathymetry (referred to with an "*a*" in the right panel of Figure 3, where colours are brown).

It is important to underline that another survey covering approximately the same area as that of Figure 3 was available for the period May-June 2017. The information resulting from the difference of such topographies, integrated with the available information on dredging activities operated during the same period allowed to reconstruct from a semi-quantitative point of view the sediment dynamics occurred during this time window of approximately one year. Such

https://doi.org/10.5194/os-2020-90
Preprint. Discussion started: 17 September 2020

information was used in the process of calibration/validation of the numerical model of sediment erosion and transport, as detailed in Sect. 5.

3.2 – Sediment data

Information on the sediment textures in the sea is usually poorly available. In this case we had access to the MArine Coastal Information sySTEm (MACISTE; http://www.apge.macisteweb.com) implemented by the Department of Science of Earth, Environment and Life (DISTAV) of the University of Genova, where the results of several chemical and physical sediment surveys are stored and accessible. Unfortunately, albeit the chemical information is comprehensive, information on the grain size is rather poor for what concerns the inner area of the port. The red dot of Figure 2 represents the only location inside the basin where the information on the texture composition and grain size was available. These characteristics are necessary for the sediment transport model, and they were used in the simulations for the entire domain of the numerical model (see Sect. 4.2).

3.3 – Naval traffic

Year 2017 was considered as a typical year from the point of view of the naval traffic in agreement with the Port Authority of Genoa and with Stazioni Marittime SpA. The traffic was available on a daily basis and it included the information on the docks of arrival/departure and the name of the involved vessels. The entire year was considered, in order to account for the typical seasonality of the traffic concentration, much more relevant for passenger vessels in the period from the end of spring to the beginning of fall.

For extra information on the characteristics of the vessels, such as length, width, tonnage, draught and typical routes inside the port during arrivals and departures we referred to the public web page https://www.marinetraffic.com.

The outcome of the analysis will be presented in Sect. 4.1.

4 – The numerical models

The non-hydrostatic version of MIKE 3 HD flow model (DHI, 2017) was used to simulate the propeller induced three-dimensional current along the port basin. The resulting hydrodynamic field was coupled with the sediment transport module MIKE 3 MT (DHI, 2019), suitable for fine-grained and cohesive material., in order to drive the erosion, advection-dispersion and deposition of fine sediment along the water column.

4.1 – The hydrodynamic model

https://doi.org/10.5194/os-2020-90
Preprint. Discussion started: 17 September 2020

MIKE 3 FM flow model is an ocean circulation model suitable for different applications within oceanographic, coastal and estuarine environments at global., regional and coastal scales. It is based on the numerical solution of the Navier-Stokes equations for an incompressible fluid in the three dimensions (momentum and continuity equations), on the advection-diffusion of potential temperature and salinity and on the pressure equation which in the present non-hydrostatic version is split into a hydrostatic and a non-hydrostatic component. The closure of the model is guaranteed by the choice of a turbulence closure formulation with different possible options amongst a constant value, a logarithmic law scheme or a k-ε scheme, which is the one used in the present implementation. The surface is free to move and it can be solved using a sigma coordinate (as it is the case in the preset study) or a combined sigma-zed approach. The spatial discretization of the governing equations of the model follows a cell-centered finite volume method. In the present implementation of the model we used the barotropic density mode, thus temperature, salinity and consequently density are constant in time and space during the simulations.

The domain of the present implementation of the model is presented in the upper panels of Figure 4. The images show two examples of computational grids used for the simulations. In these cases the docks are T1 (left panel) and T10 (right panel) during inbound operations. The grids are a combination of unstructured triangular and quadrilateral cells with horizontal resolution varying from 30 meters in the furthest areas from the ship trajectory, to 5 meters approximately within the closest area to the ships propellers. The mesh is rectangular in those areas where the ships are moving straight and the 5 meter resolution covers a corridor of approximately 50 meters of width. In the manoeuvring areas the mesh becomes unstructured and the resolution is again 5 meters. The red lines in the middle of the 5 meter resolution corridors of the upper panels represent the routes followed by the ships inside the port. The lower panels of the figure are snapshots taken from the web service https://www.marinetraffic.com showing the actual routes of the vessels birthing in the same docks as the upper panels (T1 and T10) as recorded by the AIS system mounted on the ships. As shown in Figure 4 the reconstructed trajectories of the ships in the model are realistic and fully representative of the real ones.

Table 1 shows the results of the traffic analysis within the Port of Genoa for year 2017 conducted on the traffic data provided by Stazioni Marittime SpA on a daily basis. The average lengths, widths and draughts of the ships were evaluated calculating the mean of the single quantities weighted on the number of passages occurring per year.

https://doi.org/10.5194/os-2020-90
Preprint. Discussion started: 17 September 2020

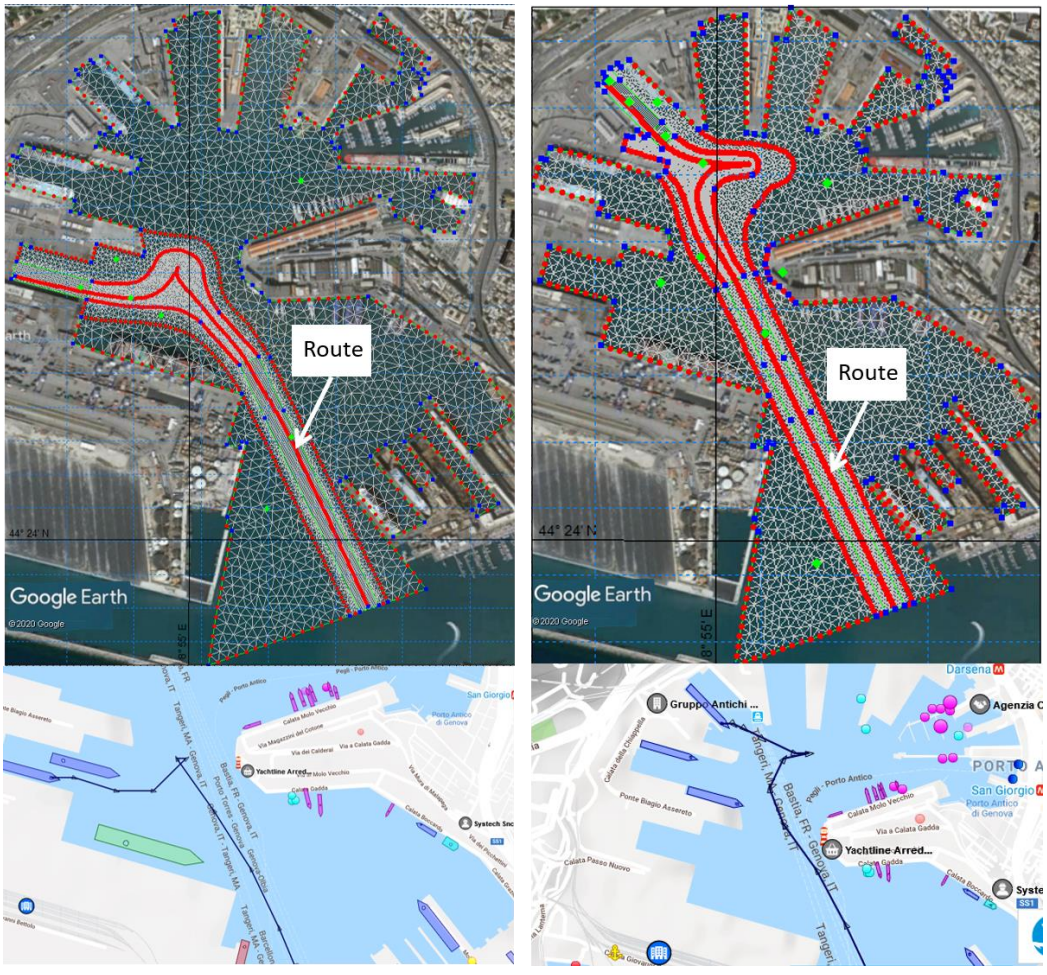

Figure 4 - Model domain and computational grids for docking routes of T1 (left panel) and T10 (right panel) docks. In the lower panels the corresponding actual routes are shown

Table 1 - Analysis of ship traffic in the port of Genoa for year 2017 and main characteristics of the ship representative of each dock. The ship's length, width, draught and propeller's diameter values are expressed in meters

Dock	Number of Berthing	% Berthing	Average Length [m]	Average Width [m]	Average Draught [m]	Average Diameter [m]
1012	122	6.4%	318.41	37.86	8.33	5.80
1003	47	2.5%	276.20	30.07	7.45	5.20
D.L.	12	0.6%	290.86	32.02	7.82	5.40
T11	123	6.4%	213.23	31.67	7.16	5.20
T10	202	10.5%	181.88	26.44	6.46	4.70
T9	8	0.4%	152.96	24.81	5.91	4.40
T7	308	16.1%	214.27	26.45	6.85	4.90
T6	291	15.2%	204.93	26.35	6.62	4.80
T5	351	18.3%	203.93	29.57	6.95	5.00

https://doi.org/10.5194/os-2020-90
Preprint. Discussion started: 17 September 2020

T3	87	4.5%	155.16	25.60	6.17	4.50
T2	202	10.5%	185.66	27.85	6.68	4.80
T1	164	8.6%	204.00	28.33	6.93	5.00
TOTALE	**1917**	100.0%	---	---	---	

In the vertical, the model is resolved over 10 sigma layers evenly distributed. The resulting layers depth vary from approximately 1 meter in the berthing areas to approximately 2 meters in the pits and in the areas closer to the port's entrance.

4.1.1 - Propeller's jet velocity

The propellers maximum jet velocity was calculated through the guidance provided in the Code of Practice of the Federal Waterways Engineering and Research Institute (Abromeit et al., 2010) and in the PIANC Report n. 180 (MarCom WG 180, 2015), basing on the German approach. The relevant parameters for the calculations are those shown in Figure 1. The maximum velocity V_0 after the jet contraction generated by the propeller is developed along the propeller's axis. For unducted propellers it is described by Eq. (1a), for propeller ratio $J=0$ (ship not moving) or Eq. (1b) for $J\neq 0$ (moving ship).

$$V_0 = 1.60 f_n n_d D \sqrt{K_T} \quad (1a)$$

$$V_{0j} = \frac{\sqrt{(J^2 + 2.55 K_{Tj})}}{\sqrt{1.4\frac{P}{D}}} V_0 \quad (1b)$$

where n_d [1/s] is the design rotation rate of the propeller, f_n is the factor for the applicable propeller rotation rate (non dimensional), D is the propellers diameter [m], K_t or K_{tj} is the thrust coefficient of the propeller (non dimensional) in the case of non-motion or motion of the ship, respectively; P is the design pitch [m]. Typical values for fn are 0.7 - 0.8 during manoeuvring activities, while the P/D ratio can be assumed approximately equal to 0.7. K_t or K_{tj} can be estimated through Eq. (2a) and (2b), according to the state of motion of the ship:

$$K_t = 0.55 \frac{P}{D} \quad (2a)$$

$$K_{tj} = 0.55 \frac{P}{D} - 0.46 J \quad (2b)$$

The propeller ratio J depends on a wake factor w varying from 0.20 to 0.45 (non-dimensional) and on the velocity of the ship according to Eq. (3):

$$J = \frac{v_{S(1-w)}}{nD} \quad (3)$$

https://doi.org/10.5194/os-2020-90
Preprint. Discussion started: 17 September 2020

As proposed by Hamill (Hamill, 1987) and further described by Wei-Haur Lam et al. (Lam et al. 2005), the downstream propeller induced jet is divided into a zone of flow establishment (closer to the propeller) and a zone of established flow (further downstream). The resulting velocity V_0 used in the model to calculate the corresponding discharge and momentum sources is considered as the maximum velocity at the beginning of the zone of the established flow.

Having no direct information on the size of the ship's propellers, reference was made to specific literature on this topic. In particular, for what concerns the propellers of Ro-Ro ferries which normally serve docks T1, T2, T3, T5, T6, T7, T9, T10 and T11, we relied on the report n° 02 of the project "Mitigating and reversing the side-effects of environmental legislation on Ro-Ro shipping in Northern Europe" (Kristensen, 2016) implemented by the Technical University of Denmark (DTU) and HOK Marineconsult ApS. According to this study the relationship between the draught and the diameter of the ferry's propeller is given by Eq. (4):

$$D_{prop} = 0.56 \times H_{draught} + 1.07 \quad (4)$$

where D_{prop} is the propeller's diameter [m], and $H_{draught}$ is the maximum draft of the ship [m]. Such relation is not valid for cruise ships having usually bigger propellers. For this type of ships, serving docks 1012, 1002 and, only partially, D.L. and T11 we relied on direct communications from operators passenger ships design sector, and double checked the information with formulas of Eq. (4) and Eq. (5), this latter valid for double propeller passenger ships. This qualitative analysis brought to the diameters presented in Table 1.

$$D_{prop} = 0.85 \times H_{draft} - 0.69 \quad (5)$$

In order to represent the propeller in a realistic way the water discharge obtained combining the diameter of the propeller and the intensity of the jet is discretized into a certain number of smaller discharges respectively associated in the numerical model to different smaller sources of momentum. The distribution of volume and momentum sources follows a Guassian (normal) distribution with a discretization step of 0.5 meters.

Figure 5 shows the representation of the propeller's induced jet in the hydrodynamic model. The left panel represents the plan of Dock 1012, where a large cruise ship is departing. The solid line of the upper left panel is the location of the vertical transect shown in the upper right image, representing the jet velocity in the plane *xz*. The dashed line in the upper left panel represents the trajectory followed by the axis of the departing ship, and the associated jet's velocity in the *yz* plane is shown in the bottom panel. Albeit the non optimal horizontal resolution in terms of propellers representation, the resulting jet appears extremely realistic both in the transverse and in the longitudinal directions.

https://doi.org/10.5194/os-2020-90
Preprint. Discussion started: 17 September 2020

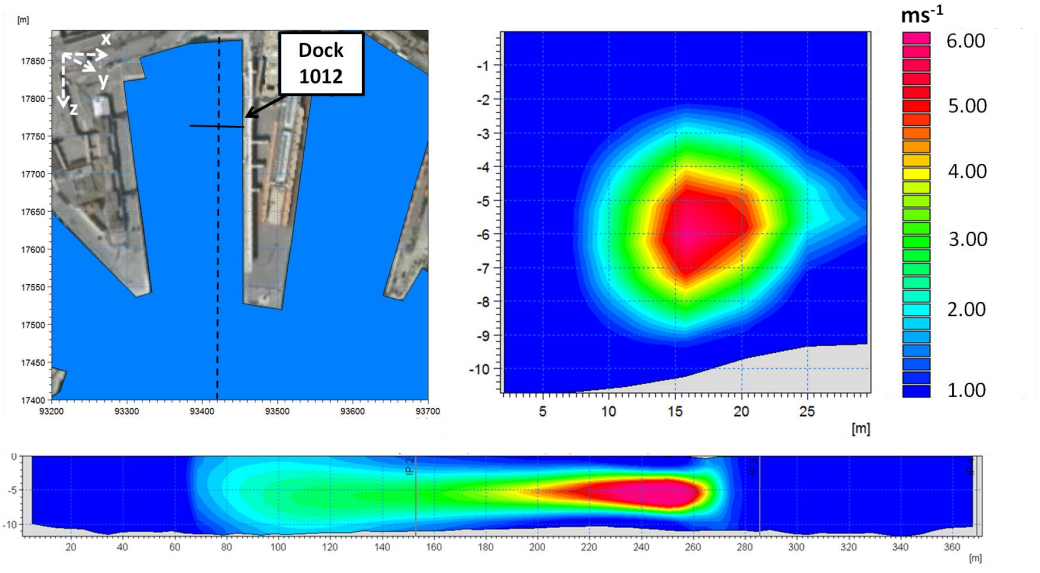

Figure 5 – Representation of the propeller-induced jet of the most representative ship departing from Dock 1012. Left: plan view; the dashed line represents the trajectory followed by the axis of the undocking ship, the solid line represents the position of the vertical transect shown in the upper right panel, showing the jet's induced velocity in the *xz* plane (propeller's plane). Lower panel: transect of velocity along the propellers axis (*yz* plane). Velocities are in ms^{-1}

In order to preserve the water mass budget we associated a sink to each source. Sinks are prescribed in terms of negative equivalent discharge (m^{3}s^{-1}) in the adjacent grid cell to the one hosting the source, in the direction of the ship motion (sinks precede corresponding sources).

The choice of the vertical and horizontal resolution of the hydrodynamic model was the result of a thorough sensitivity analysis to the grid's cells dimension. We assumed that the most appropriate resolution for the model is the one that allows the maximum (jet centreline) current produced by the combined discharge and momentum sources in the model to reach the input maximum velocity V_0. For the sensitivity analysis we considered a 4-meter diameter propeller with rotation rate of 2 rounds per second (rps) at full power. According to Eq. (1b), such a configuration results in a V_0 of approximately 6 ms^{-1} at the depth of the propeller's axis once the jet is fully developed. To this purpose, we set up an experimental configuration domain, 100 meters wide and 500 meters long. The different horizontal resolutions tested were 20 m, 10 m, 5 m, 2 m and 1 m, while for the vertical we considered two configurations: 10 and 20 layers in a constant bathymetry of 20 meters. The input value of the jet current to the model was 6 ms^{-1}.

https://doi.org/10.5194/os-2020-90
Preprint. Discussion started: 17 September 2020

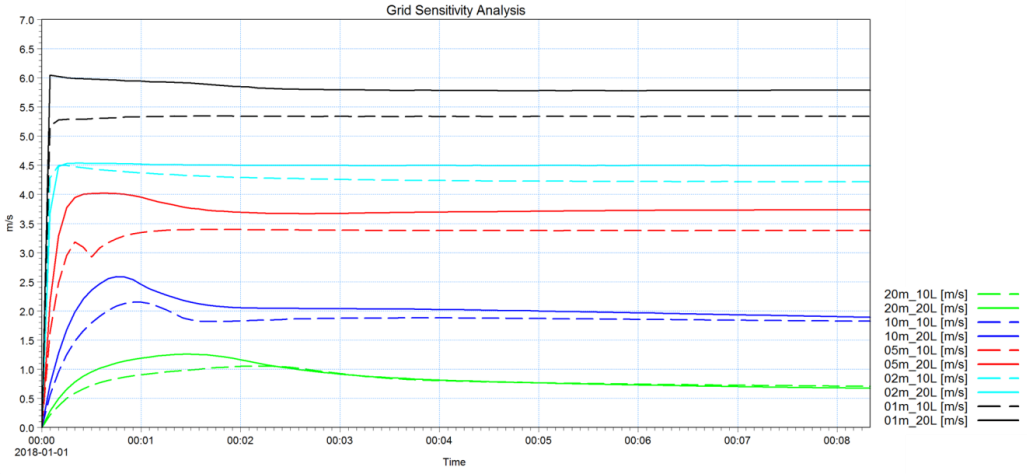

Figure 6 – Model grid sensitivity analysis to the cells dimension. The different colors correspond to the different horizontal resolution. Dashed lines indicate the configurations with 10 layers while solid lines indicate those with 20 layers

Figure 6 shows the sensitivity analysis to the grid resolution. The resulting velocity at the propeller's axis is proportional to the resolution, both in vertical and in the horizontal: the higher the resolution, the higher the resulting velocity. The most appropriate grid would be the one with 1 meter resolution and 20 vertical layers, which is the only configuration of the model which allows the jet to reach the maximum speed imposed as input. However, this configuration would require approximately one year of computational time to run the 24 simulations implemented for this study in the same computational configurations, which is obviously unrealistic. We thus looked for a compromise between acceptable computational demand and realistic resulting velocity. The final configuration was the one with 5 meters as horizontal resolution and 10 vertical levels. Since such resolutions would not allow the complete development of the current speed we introduced a correction to the input velocity of each simulated vessel by increasing it of the necessary amount to reach the empirically calculated V_0. This implied considerable additional time for manual calibration.

4.1.2 – Forcing and boundary conditions

Due to the nature of the processes of interest the only forcing accounted for is the propeller of the vessels. In fact, the jet induced by its motion is of the order of magnitude of several meters per second in the surrounding of the blades, and it has a length of influence of at least 40-50 times the propeller's diameter behind the ship (Verhei, 1983). Natural forcing such as wind, density gradients or tides are one to two orders of magnitude smaller in this area, thus they can be neglected without introducing errors potentially impacting on sediment resuspension from the bottom. On the contrary, Bernoulli wake might be responsible for currents of comparable intensity (Rapaglia et al., 2016), albeit smaller, and it

https://doi.org/10.5194/os-2020-90
Preprint. Discussion started: 17 September 2020

would be worth to be considered as a forcing of the system. In this study, though, we neglected it due to technical complications and time obligations. It will be interesting to include such process in further developments and to analyse the impact on the overall dynamics of ship induced sediment transport. However, the satisfying final results of the present work suggest that the governing processes for these dynamics are associated to propellers induced currents more than to the motion of the ship itself, likely due to the limited vessels speed in this inner part of the harbour and to the relatively large volume of water available for each passing vessel.

The boundaries of the hydrodynamic domain are the docks all around the basin and the port entrance, which is the only open boundary. Here we imposed a Flather condition (Flather, 1976) assuming constant zero velocities and levels. Such a choice allowed to minimize the boundary effects, albeit some interference between the flux and the boundary line is present (not shown). However, due to the distance between the open boundary line and the berthing areas such effects do not influence the results of the study. A zero normal velocity was imposed along the closed boundaries.

4.2 – The sediment transport model

The hydrodynamic model was coupled with a sediment transport model – MIKE 3 MT FM - valid for fine-grained and cohesive sediment (diameter smaller than 63 µm, Lisi et al., 2017). This type of sediment is mostly present in the port of Genoa and particularly relevant for the erosion, transport and further deposition, since its small dimension and weight favour relevant resuspension and advection around the basin.

The governing equations of the mud transport model are based on the advection and dispersion (AD) of the concentration of the sediment along the water column and they are detailed in APPENDIX A2. The AD equation is solved using an explicit, third order finite difference scheme called ULTIMATE (Leonard, 1991).

The model accounts for two compartments: a water and a seabed environment. The seabed is represented through a multi-bed layer and multi-fraction approach in which the different layers can exchange mass and only the top level is active, thus available for erosion. The different layers are defined through the fractions of sediment they're composed of, the degree of consolidation of the sediment within each layer, and the thickness of the single layer. The different sediment fractions are described through their associated physical characteristics, and they are eroded and deposited proportionally to their concentration both in the bed texture and along the water column. Within the water environment, the model includes flocculation processes when exceeding a certain threshold of concentration (here assumed equal to 0.01 gl-1) and hindered settling according to Wintwerp (Winterwerp and Van Kesteren, 2004) definition with a threshold of 10 gl-1. The deposition of the sediment is based on a Teeter (Teeter, 1996) profile and the threshold for deposition used was 0.07 Nm^{-2}. The sediment grain diameter is defined through the associated settling velocity, based on Stokes law. In the interface between the water and the bottom the sediment may be eroded following the approach by

https://doi.org/10.5194/os-2020-90
Preprint. Discussion started: 17 September 2020

Partheniades (Partheniades, 1965) for consolidated sediment or that by Parchure and Metha (Parchure and Metha, 1985) for soft or unconsolidated sediment. In both cases the sediment is eroded and injected into the water column when the shear stress resulting from the current, the wave action or a combination of both exceeds a certain critical value. In the present case waves were not considered since we are inside the port.

The specific equations and parameterizations referred to in the sediment model are summarized in APPENDIX A2.

4.2.1 - Sediment characteristics

Three different sediment surveys were carried out between June 2009 and July 2010. Table 2 presents the results of the surveys in terms of percentage and class of sediment per survey (last and central column, respectively). Given the nature of the study we are interested in mud and fine sand, thus the part of the texture coarser than 2 mm was not taken into consideration.

Table 2 - Sediment size data inside the port (see station identified with the red dot of Figure 2). Three different surveys were carried out between June 2009 and July 2010

Date of survey	Sediment Size	%
2009-06-15 16:00:00	Ø < 63 µm	82.4
2009-06-15 16:00:00	63µm < Ø < 2mm	16.2
2009-06-15 16:00:00	Ø > 2 mm	1.4
2009-07-15 16:00:00	Ø < 63 µm	89.2
2009-07-15 16:00:00	63µm < Ø < 2mm	9.1
2009-07-15 16:00:00	Ø > 2 mm	1.7
2010-07-28 09:00:00	Ø < 63 µm	78.2
2010-07-28 09:00:00	63µm < Ø < 2mm	17.7

We assumed that the fraction of the samples with Ø < 63 µm was composed by two grain sizes with diameters of 30 μm and 50 μm respectively, while for the observed component with diameter in the range of 63μm to 2 mm we assumed the diameter of 100 μm would be representative for the present study.

The three fractions chosen were distributed into three active bed layers. The percentage of the fine fractions amongst the texture of sediment was assumed to decrease proportionally to the depth of the layers. Thus, the first layer contained 80% of fines (specifically 50% of grains with Ø=30 μm and 30% with Ø=50 μm) and 20% of coarse (Ø=100μm), while the third layer contained 50% of coarse (Ø=100μm) and 50% of fines (specifically 20% of grains with Ø=30 μm and 30% with Ø=50 μm). In the mid layer an even distribution was assumed among the three fractions. The thickness of the three layers is 0.5 mm, 1 mm and 50 mm at the beginning of each scenario. The first layer is composed by very soft mud since it is the result of the newly deposited and finer mud. The other two layers are more consolidated and thicker, since they are harder to be eroded and they are shielded by the upper layers. The adopted description of the bottom with

https://doi.org/10.5194/os-2020-90
Preprint. Discussion started: 17 September 2020

different layers and fractions of sediment allowed to represent the port bed in a complex and comprehensive way, including the different degree of consolidation of the layers and the resulting different response to shear stress solicitations.

A summary of the most relevant characteristics of the layers and sediment fractions implemented in the sediment transport model is presented in Table 3.

Finally, potential sediment input might come from six minor streams inflowing in the port area. They have very modest basins - approximately 1 km^2 on the average – and they have been ceiling-covered for long time, acting now more as sewage collectors than as natural streams. An estimate of their contribution to the sedimentary dynamics of the port of Genoa has been conducted and the annual sediment supply to the port basin from each stream has been evaluated referring to the method proposed by Ciccacci et al. (Ciccacci et al., 1989). The estimated contribution of sediment resulted in only a few hundreds of cubic meters per year in the worst cases, which corresponds to a few millimetres of annual accumulated sediments in the surrounding of the river inlet to the wet basins. Such amount of solid matter has not been considered in the model since the erosional and depositional processes induced by the propellers' activity are higher by one or two orders of magnitude.

Table 3 – Summary of sediment characteristics as implemented in the mud transport model

Parameter	**Layer 1**	**Layer 2**	**Layer 3**
Layer thickness (mm)	0.5	1	50
Type of Mud	soft	hard	hard
Dry density of bed layer (kgm^{-3})	180	300	450
Parameter	**Fraction 1**	**Fraction 2**	**Fraction 3**
Φ (μm)	30	50	100
% of fraction in layer 1, 2, 3	50, 33, 20	30, 33, 30	20, 33, 50
W_s (mms^{-1})	0.7	2.2	8.8
τ_{ce} (Pa)	0.15	0.25	0.5
τ_{cd} (Pa)	0.07	0.07	0.07
C_{floc} (gl^{-1})	0.01	0.01	0.01
C_{hind} (gl^{-1})	10	10	10
ρ_s (kgm^{-3})	2650	2650	2650

5 - Results

The most representative results of the hydrodynamic and sediment transport model are presented in this section. Due to the large number of simulations carried out, only those regarding two docks are shown. However, the results not shown corresponding to the other simulations are similar in terms of hydro and sediment dynamics. The results discussed are those of the simulations of docks 1012 and T7. Dock 1012 is particularly important since it hosts the biggest passenger vessels operating in the port, while dock T7 is particularly relevant due to the high frequency of passages.

https://doi.org/10.5194/os-2020-90
Preprint. Discussion started: 17 September 2020

Figure 7 shows the propeller's generated current in the bottom layer and at the depth of the propeller's axis (upper right and left panels, respectively) and the resulting suspended sediment concentration in the same layers (corresponding lower panels) during the departure of a cruise vessel from dock 1012. The characteristics of the vessel representative of the traffic of the dock are those of Table 1. When departing, the engine is operated close to full power, which we assumed to result in a rotation rate of 2 rounds per second (rps) for the propeller. This induces a maximum velocity at the depth of the propeller axis close to 9 ms^{-1} which is damped to approximately 2 ms^{-1} on the bottom of the berthing basin along the vessel's route. Such intense jet is deflected to the left due to the head wall of the berthing basin which constrains the flow and induces a cyclonic eddy, well developed along the whole water column. The cone-like envelop of the jet in the vertical plane as sketched in the theoretical scheme of Figure 1 is appreciable from the upper panels of Figure 7, which refer to the same instant: the influence of the propeller on the bottom occurs several tens of meters behind the propeller's position, and the velocity at the bottom is strongly reduced. The induced eddy in the wet basin acts as a trap for the eroded sediment, which enters the cyclonic gyre (or anti-cyclonic in the case of departure from the opposite dock) and tends to deposit in the middle of the basin, where the fluxes progressively decrease. The position of the eye of the cyclone evolves parallel to the docks' longitudinal walls and induces the sediment trapped inside the gyre to sink along the longitudinal axis of the wet basin. Such dynamic occurs similarly for all the horseshoe-shaped wet basins, inducing accumulation along the central portions. The re-suspended sediment may reach very high concentrations in the bottom layers, up to several hundreds of mgl^{-1}, depending on the different specific characteristics of the sediment texture (mainly grain size, level of compactation, availability to erosion) and of the vessel (mainly dimension of the propellers, rotation rate, draught).

Different hydro and sediment dynamics occur during the inbound phase of vessels manoeuvring inside the port. The majority of the manoeuvring operations (i.e. when vessels rotate within a turning basin and proceed backwards to the docks) occur in the turning basins delimited by the dashed circles *a* and *b* shown in Figure 2. When starting the manoeuvre, engines operate to high power in order the allow the rotation of the ship. Within these operations the vessel's longitudinal axis rapidly changes direction (order of tens of seconds up to a few minutes) spanning wide angles according to the specific manoeuvre to be undertaken. The propellers induced jet follows the same rotation along the horizontal plane resulting in a fan-like distributed set of directions for the associated currents. Such operations are represented by the model in a realistic way as shown in Figure 8, which refers to the berthing of vessel representative of dock T7. The currents shown in the figure are those associated to the propeller's axis during four different moments of the turning manoeuvre. Each panel refers to a time interval of approximately 100 seconds from the previous one. The successive instants are presented in the order up-left, up-right, down-left and down-right, respectively. In the lower-right panel the propeller has already changed direction of rotation and the vessel is now proceeding backwards. The

https://doi.org/10.5194/os-2020-90
Preprint. Discussion started: 17 September 2020

induced current jet is thus heading towards the centre of the port, pushing the sediment towards this area. What simultaneously happens at the seabed is shown in Figure 9. Albeit the jet induced currents are very much weaker at the seabed than those at the depth of the propeller's axis, they are still relevant and may reach intensities up to 1 ms^{-1}, depending on the local bathymetry.

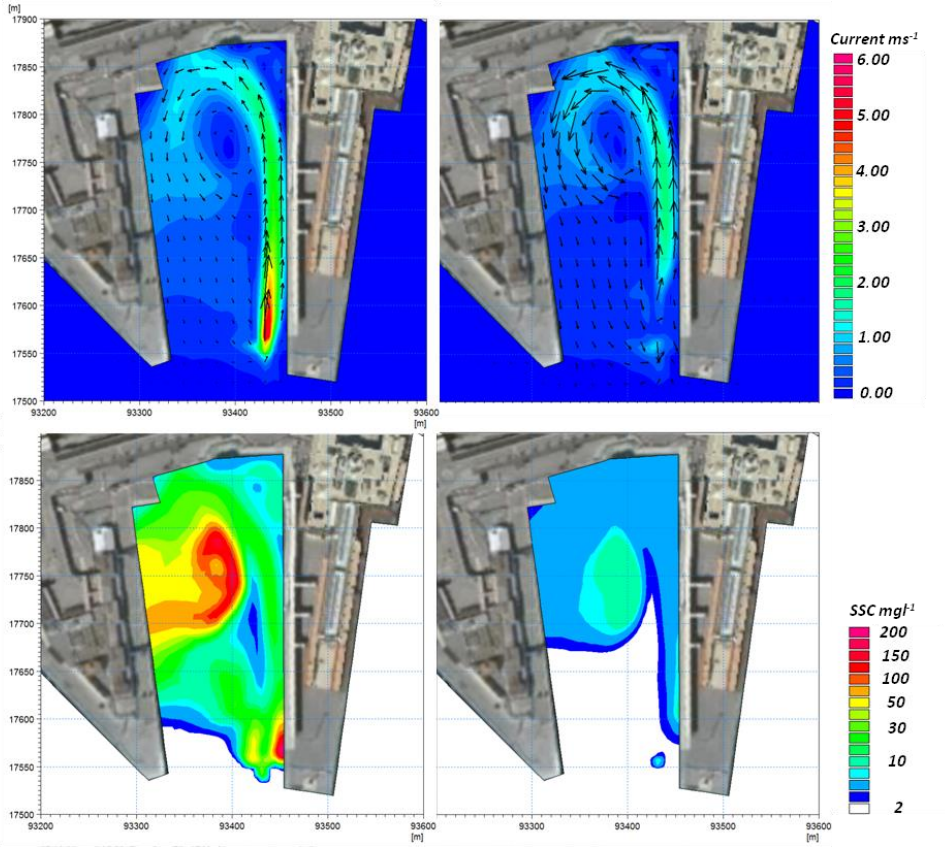

Figure 7 – Results of the numerical models. Upper panels: current intensity and direction in the bottom layer (right) and in the layer corresponding to the axis propeller. Lower panels: resulting suspended sediment concentration (SSC, mgl^{-1}) in the same layers as the upper panels. The images refer to the undocking of the cruise vessel representative of dock 1012.

The current distribution at the seabed is much more chaotic than at the propeller's axis depth. It is to be noted that this area of the port corresponds to the natural pit (which reaches 22 meters below the surface in the deeper part, approximately) where the material dredged from accumulation areas is normally dumped during the sea bottom maintenance activities. The dashed line shown in the lower-right panels of Figure 8 and Figure 9 refers to the transect

https://doi.org/10.5194/os-2020-90
Preprint. Discussion started: 17 September 2020

presented in Figure 10, in the same instant (i.e. when the vessel has ended the manoeuvre in the circle *b* and is approaching dock T7 backwards).

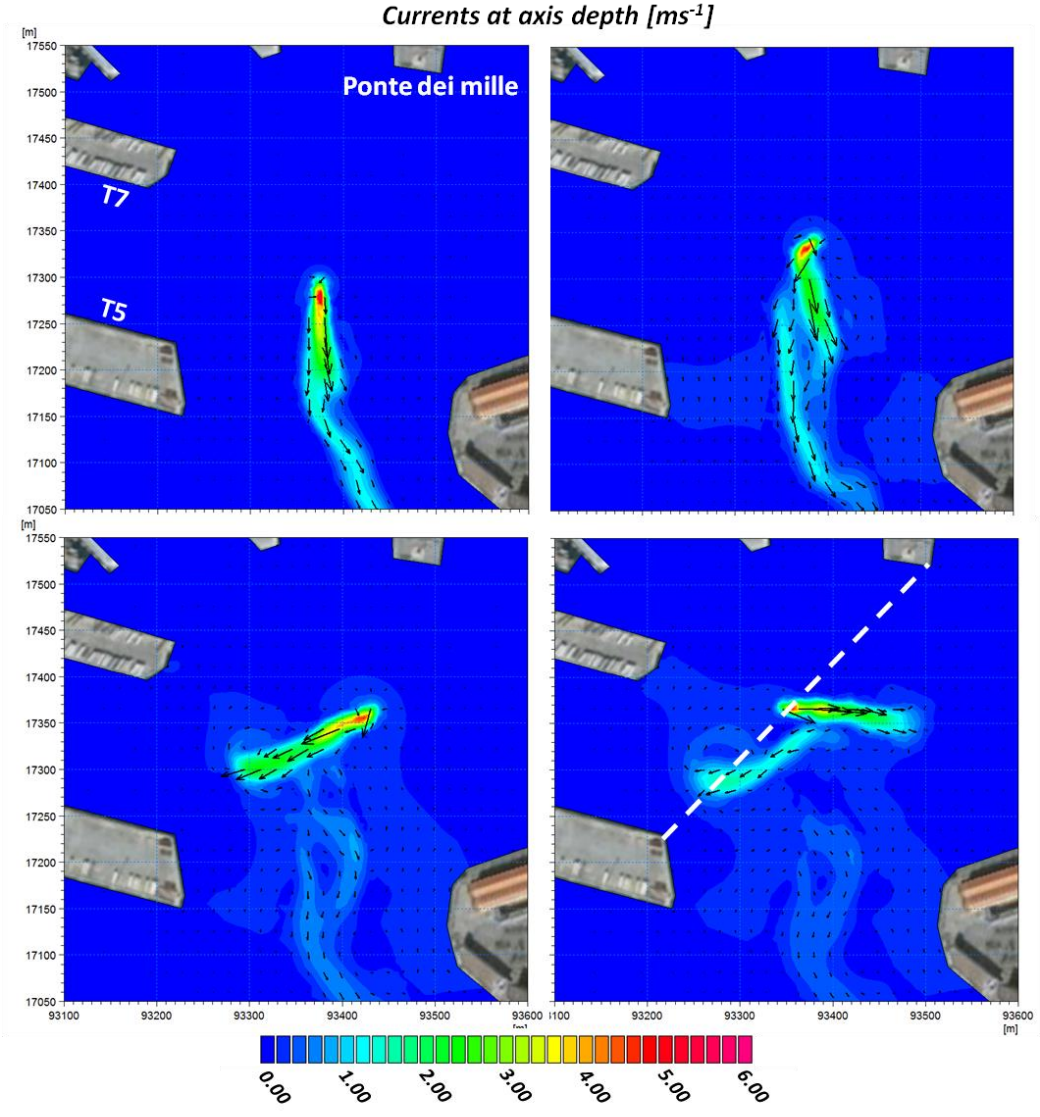

Figure 8 – Results of the hydrodynamic model at the depth of the propeller's axis. Each panel refers to a time interval of approximately 100 seconds from the previous one. The temporal order of the panels is up-left, up-right, down-left and down-right

https://doi.org/10.5194/os-2020-90
Preprint. Discussion started: 17 September 2020

449 A combined analysis of Figure 8, Figure 9 and Figure 10 helps understand the dynamics occurring in the turning basin *b*
450 during manoeuvres to approach docks T5, T6 and T7. This is particularly important in order to understand the overall
451 sediment dynamics of the entire port since these three docks operate approximately half of the entire passenger traffic.
452 The propeller's induced velocities at the bottom of the natural pit during turning manoeuvres is variable and may
453 exceed 1 ms^{-1}, which is a relevant current intensity able to entrain and move a large amount of sediment. The resulting
454 re-suspended sediment concentration may reach important values, exceeding 50-60 mgl^{-1}, as shown in the lower panel
455 of Figure 10. Once re-suspended from the pit, the sediment is advected around by the jet induced complex field of
456 currents of Figure 8 and Figure 9. This area is normally refilled with freshly dredged material resulting from the seabed
457 maintenance activities, thus the propeller's induced currents on the bottom have an enhanced effect of erosion on the
458 unconsolidated material and are able to rapidly nullify the benefit of the dredging operations. In this regard, the results
459 of the simulations suggest to avoid to use the natural pit as a dumping area for the resulting material of such activities
460 and prove that integrated modelling can be a fundamental tool for the comprehension of the processes and mechanisms
461 related to sediment transport and for an optimized planning of maintenance activities.
462

https://doi.org/10.5194/os-2020-90
Preprint. Discussion started: 17 September 2020

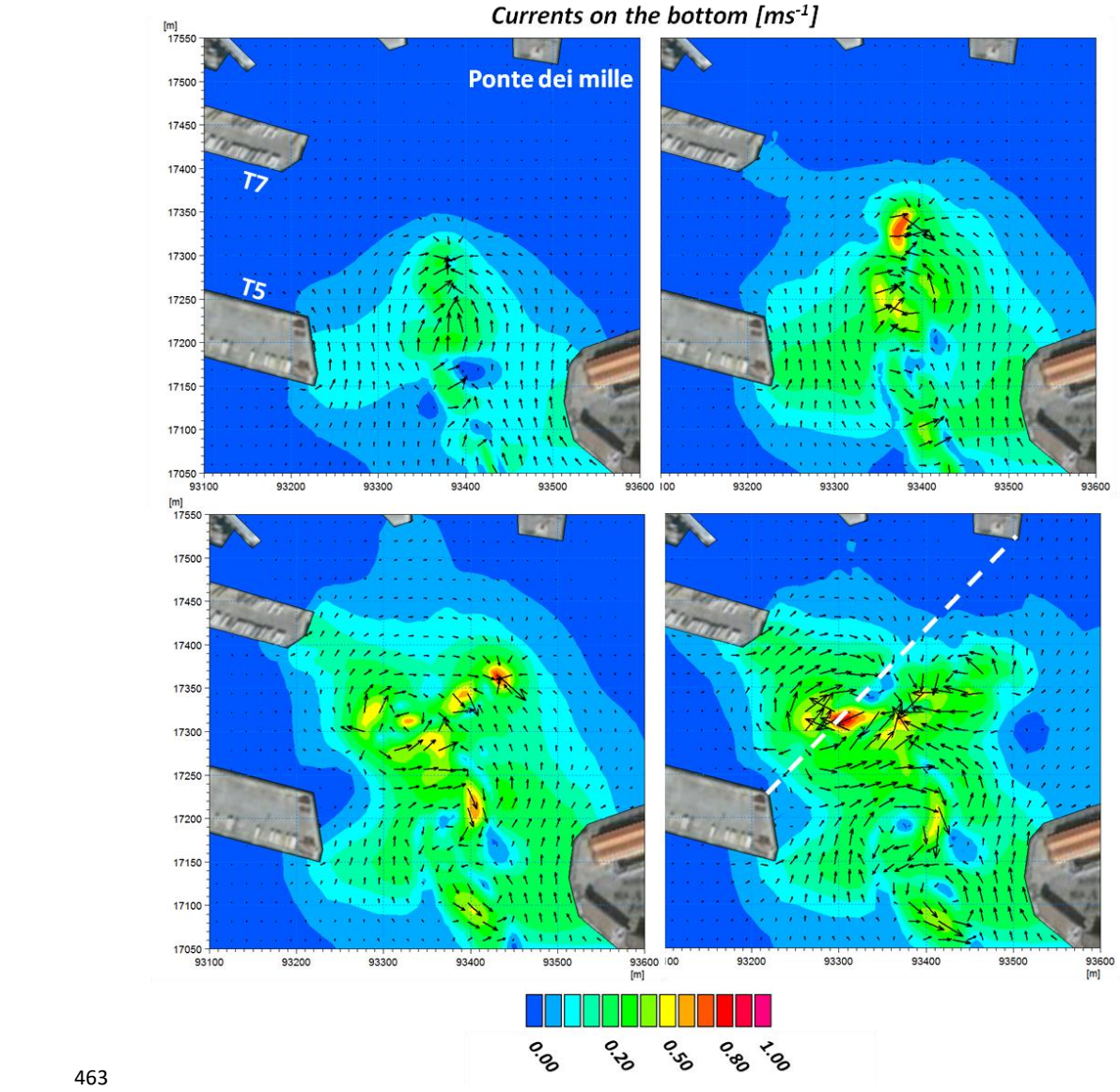

463

464 **Figure 9 – Same as Figure 8 but for the bottom layer**

465

466

https://doi.org/10.5194/os-2020-90
Preprint. Discussion started: 17 September 2020

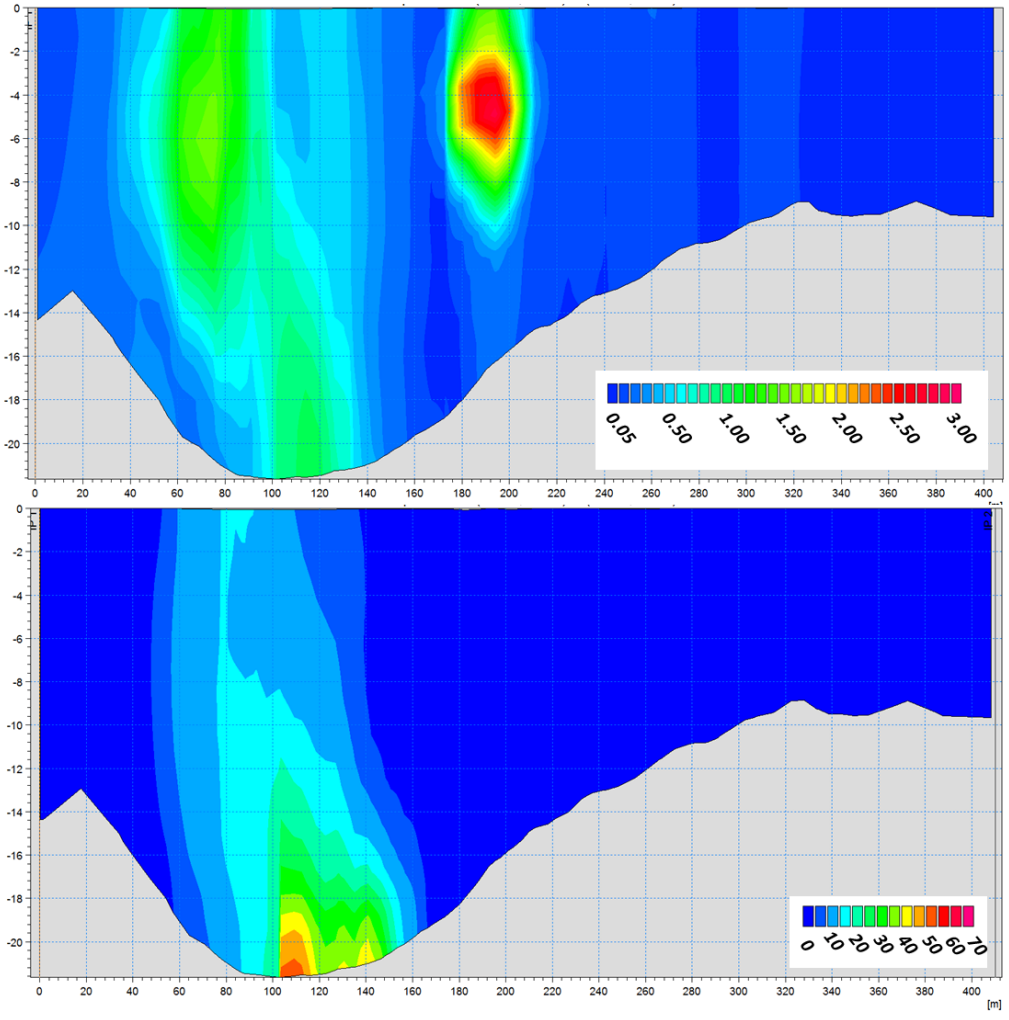

Figure 10 – Velocity intensity in ms^{-1} (upper panel) and sediment concentration in mgl^{-1}(lower panel) along the transect from the head of *Ponte Assereto* to the head of *Ponte dei Mille*

The impact on the bed thickness due to the naval traffic is depicted in Figure 11, which presents the erosion and deposition maps resulting from the simulations of one departure (left) and one arrival (right) of the representative passenger vessels of docks 1012 (up) and T7 (down). The blue colors represent areas of erosion, while the red colors represent those of accumulation of the sediment after an interval of time sufficiently long for the re-suspended sediment to completely settle down. It is evident from the left panels of the figure that during the vessel's departure a considerable amount of material tends to be eroded from the basement of the docks and settles in the center of the mooring basins. This mechanism is clearly related to the vessel's departure (left panels) rather than to the vessel's arrival (right panels). The erosion underneath the vessel's keel along the ship's trajectory is well evident both during

https://doi.org/10.5194/os-2020-90
Preprint. Discussion started: 17 September 2020

departure and arrival., in agreement with experimental literature findings (Castells et al. 2018). The order of magnitude of erosion and deposition of one single vessel's passage is of a few millimeters in the areas most influenced by the vessel's activity.

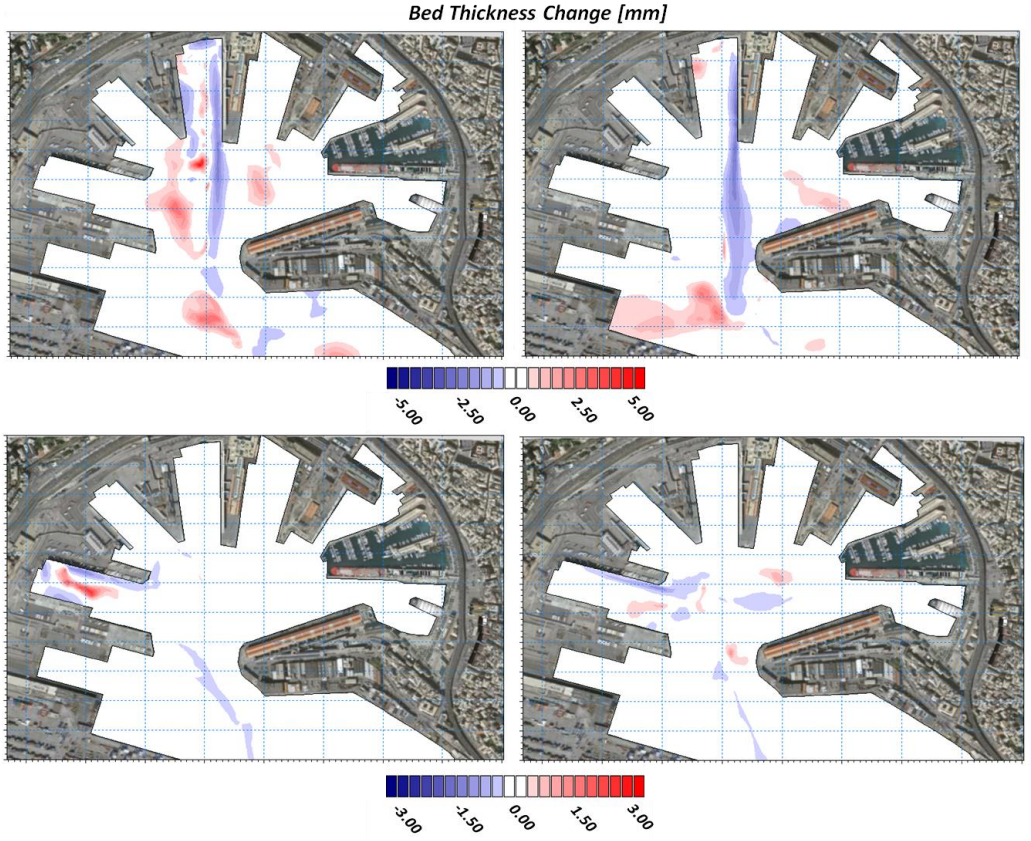

Figure 11 – Erosion and deposition maps resulting from one departure (left) and one arrival (right) of the representative passenger vessels of docks 1012 (up) and T7 (down)

Such impact might become a real threat for the continuity of the operability of large and busy ports like the Port of Genoa in the medium and long timescales. The few millimeters of accumulation and erosion might become several tens of centimeters after a few thousands of annual passages. Relying on the traffic analysis of Table 1 we projected each single naval passage to a one-year period and superimposed the effects of erosion and deposition of the vessels representative of all the passenger docks. We were thus able to reconstruct the annual port seabed evolution for year 2017. The effects of the single passages were weighted by the occurrences of the year 2017, thus obtaining 24 maps (one for each docking and one for each undocking), and the results of the 24 maps were integrated to obtain the final

https://doi.org/10.5194/os-2020-90
Preprint. Discussion started: 17 September 2020

map. To take into account the fact that the trajectories to reach a dock (or to depart from it) slightly vary from passage to passage, a Bartlett spatial filter was applied to the integrated results using the values 4, 2 and 1 as weights. Figure 12 presents the results of this analysis. In the left panel the results from the modeling system in terms of annual erosion (blue) and accumulation (red) are shown, while in the right panel the observed seabed evolution is shown. The observed map was reconstructed through the results of two different bathymetric surveys carried out in the periods May-June 2017 and March-June 2018. The difference of the bathymetries of the two surveys resulted in the evolution of the seabed during the approximate period of one year, except for dredging operations. We used numbers in the maps to indicate areas where the most relevant dynamics outlined by the study take place.

It is to be noted that the area between the head of *Ponte dei Mille* and the head *of Molo Vecchio* identified as 1 was dredged during the period October-December 2017 and approximately 15.000 m^3 of solid material were removed and dumped into the natural pit of the port, here indicated with number 5. Consequently, what appears at first sight from observations as an area of erosion due to the vessel traffic - area 1 in the right panel of Figure 12 - is actually an area of accumulation, as it is also confirmed by the fact that dredging operations were conducted. Similarly, the accumulation observed in area 5 (right panel of Figure 12) is not the result of the induced action of the propellers, but it is the result of the accumulation of the sediment dumped after maintenance dredging operations. The model results are in total agreement with these dynamics. As discussed above, the material re-suspended during vessels' maneuvers is likely pushed towards area 1 during the phase of backward advancing of the vessels when approaching the docks. On the contrary, area 5 is partially an area of erosion, as evidenced by the model. The freshly deposited material during dredging operations is thus soon re-suspended.

https://doi.org/10.5194/os-2020-90
Preprint. Discussion started: 17 September 2020

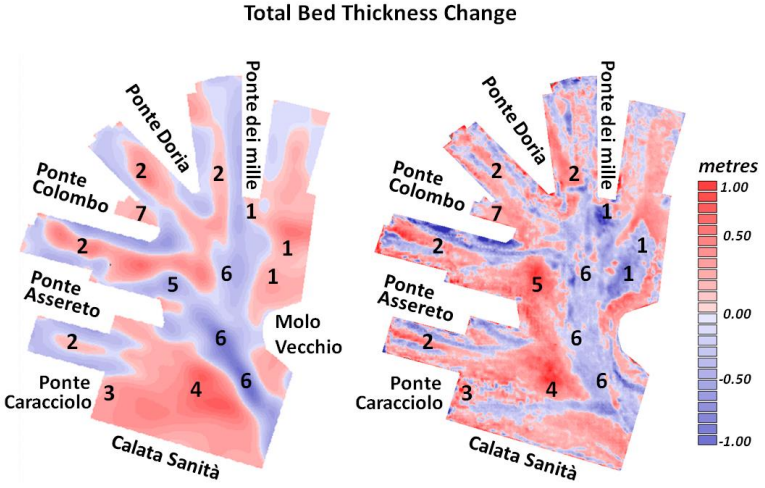

510

511 **Figure 12 – Annual erosion and deposition map reconstructed on the basis of the hydrodynamic and sediment**
512 **transport simulations for the year 2017**

513 Area 1 accounts for approximately 30-40 cm of accumulated material per year, with local maxima of up to 50 cm.
514 Similar values were estimated against years of managing experience by personnel of Stazioni Marittime S.p.A (personal
515 communication).

516 The central portions of the wet basins marked with number 2 in Figure 12 are areas of deposition, mainly due to the
517 phase of departure of the ships. Again, the model is able to well reproduce both the accumulation along the central parts
518 of the basins, where it may reach 20 cm per year or even more, and the erosion along the walls of the docks. Here the
519 propellers erosive action might result in issues for the stability of the docks, especially along those of dock 1012, where
520 the biggest cruise vessels operate.

521 The erosion underneath the vessels' typical routes (i.e. from the entrance to approximately the center of the port) is also
522 well represented by the model, and it is identified in the figure with the number 6. Good agreement between the model
523 and the observations is also evident in the deposition area identified with the number 7, where a local gyre forms and
524 entraps the suspended sediment. Finally, also areas 3 and 4 are subject to deposition, and qualitative agreement between
525 the model and the bathymetric differential survey is evident from Figure 12. The erosive print observed in the survey
526 under these areas is most likely due to activities related to cargo vessels when approaching and departing from dock
527 *Calata Sanità*. This latter was not object of the study, which was intended only for passenger docks whereas *Calata*
528 *Sanità* operates only container ships, thus the model does include the naval traffic here.

529 In general., the comparison between the observed and the modeled annual evolution of the port seabed shows a very
530 good agreement, it proves the reliability and robustness of the hydrodynamic and sediment transport model and it

https://doi.org/10.5194/os-2020-90
Preprint. Discussion started: 17 September 2020

finally shows the potential importance of an integrated modeling approach to optimize the management of the port activities.

5 – Summary and Conclusions

The impact of naval traffic on the seabed of the passengers Port of Genoa was investigated by means of numerical modeling. The combination of a very high resolution, non-hydrostatic, circulation model (MIKE 3 HD FM) with a sediment transport model (MIKE 3 MT FM), based on unstructured grids on the horizontal and on sigma levels on the vertical allowed to reconstruct the annual evolution of the port seabed. The final results of the modeling in terms of maps of erosion and deposition inside the basin were qualitatively supported by observational evidence. The approach followed was to simulate only one arrival and one departure from each dock of the port and to analyze the impact of a single naval passage on the seabed in terms of sediment concentration, motion and distribution.

Following the traffic analysis in the port for a typical year (year 2017) the detailed situation of the number of arrivals and departures for each dock was available as a starting point for the study. Through the superimposition of the single effects of the traffic weighted for the annual number of passages of the most representative vessel operating on each dock the annual map of erosion/deposition was reconstructed and validated on a semi-quantitative basis versus differential bathymetric surveys available for the same period.

In general., the simulations showed that the velocity intensities on the bottom induced by propeller's generated jets may reach almost 2 ms^{-1}, mainly depending on the dimension of the propellers, on the rotation rate and on the distance between the propeller and the bottom. Such velocities may reach up to 8-9 ms^{-1} at the propeller's axis depth, and penetrate horizontally through the water for long distances, up to at least 40-50 times the propeller's diameter. The bed shear stresses induced by these velocities, as well as the propeller jet induced entrainment mobilize and re-suspend high amounts of the fine and less compacted sediments present inside the port. Fine fractions with smaller fall velocities tend to remain in suspension for longer periods of time, resulting in creation of sediment plumes. Hong et al. (2016) have shown in their laboratory test results the dependency of the concentration profiles behind propeller jets to sediment grain size distribution, amongst other parameters.

The final findings showed how relevant the deposition rates might be in a densely operated port, reaching values of several tens of centimeters per year in some local areas.

The type of approach we adopted was particularly useful not just because it allowed to minimize the computational time, but also because it allowed to decompose the overall complex picture of sediment transport of the entire port into several simpler pictures. Consequently, the analysis of the single hydro and sediment dynamics occurring for each dock and vessel was possible as well as the identification of the specific routes responsible of the particular problems of

https://doi.org/10.5194/os-2020-90
Preprint. Discussion started: 17 September 2020

562 erosion and accumulation historically reported by the managing authorities of the port operations and traffic. The range
563 of current intensities induced by the propellers action was identified along the water column, and it can be further used
564 as a solid and scientific-based benchmark value for potential defensive actions for the seabed and port structures that
565 might be undertaken in the future in order to preserve the port's full operability.
566 The most relevant mechanisms regarding the port hydro and sediment dynamics occurring during vessels passages were
567 identified and the following analysis allowed to understand how and why specific areas are subject to erosion and other
568 areas are subject to deposition, and to what extent these mechanisms occur. In particular, the mechanism of erosion
569 ongoing along the docks walls and that of deposition along the central portions of the mooring basins were identified
570 and explained, as well as the deposition process constantly ongoing in the area confined between the head of *Ponte dei*
571 *Mille* and the head of *Molo Vecchio*. This last process was particularly important to reproduce and understand for the
572 port managers since it occurs at a very important rate, up to 40-50 cm per year in some local areas. Finally, the natural
573 hole located off the heads of *Ponte Colombo* and *Ponte Assereto* was identified through the model as an area of erosion,
574 albeit its relevant depth. This is mainly due to the turning maneuvers carried out by vessels in this area which partially
575 corresponds to one of the turning basins of the port and which involves approximately the 50% of the entire traffic of
576 the port (docks T5, T6 and T7). Since such location has been historically used as a dumping site for the resulting
577 material of seabed maintenance dredging, the study showed how unfit this area is for such purpose, since the freshly
578 deposited sediment is soon re-suspended by the intense currents induced by the vessels turning operations.
579 The importance of this study was not only to prove how integrated high resolution modeling might be able to reproduce
580 the most relevant and complex mechanisms of hydrodynamics and sediment transport occurring inside ports – which
581 was however done successfully – but it was also to suggest, once its reliability was proven, that it can be used as a
582 fundamental tool for an optimized port management. In fact, it could be used to regulate the naval traffic in ports in
583 order identify the most suitable schedule and routing in terms of sediment concentrations, bottom velocities, erosion and
584 accumulation. Or again it could be used to identify the biggest vessels potentially operating in the docks for the
585 planning of the future commercial traffic, or to study the impact of the increasing traffic of ports on the seabed and on
586 the ports structures, or finally for an awareness planning of the recurring dredging operations related to the sediment
587 accumulation problems that the majority of densely operating ports must regularly face, most of the times without being
588 correctly prepared.
589 Daily fully-operational implementations of similar integrated systems are also possible to set up, since the daily
590 schedule of the port is known. This would allow to continuously monitor the evolution of the seabed and to be
591 constantly and fully aware of the potential criticalities to face.

https://doi.org/10.5194/os-2020-90
Preprint. Discussion started: 17 September 2020

592 An important process that should be included in the future developments of the present study is the effect on the
593 sediment resuspension, advection and dispersion due to Bernoulli wake and its combination with the propeller's
594 induced jets. This mechanism was not included in the present version of the system. The current intensities caused by
595 vessels' generated waves during and after their passages are surely smaller than those induced by propellers along their
596 axis, but they tend to penetrate along the water column and reach the bottom carrying a significant amount of energy,
597 and possibly re-suspending important amount of solid material (Rapaglia et al.2011), probably enhancing the vertical
598 mixing and maybe inducing the sediment to be suspended for longer periods and at higher depths.
599
600

601 **APPENDIX A1 – Hydrodynamic model governing equations**

602 MIKE 3 Flow Model FM is based on the Navier-Stokes equations for an incompressible fluid under the assumptions of
603 Boussinesq. The governing equations of the model are the equations of momentum (A1.1) and mass continuity (A1.2),
604 the equations of heat and salinity transport (A1.3 and A1.4, respectively) and the equation of state (A1.5) based on the
605 UNESCO formula of 1981 (UNESCO, 1981a). Considering a Cartesian coordinate system *(x,y,z)* we have:

606 $$\frac{\partial u}{\partial x}+\frac{\partial v}{\partial y}+\frac{\partial w}{\partial z}=0 \quad \text{(A1.1)}$$

607

608 $$\frac{\partial u}{\partial t}+\frac{\partial u^2}{\partial x}+\frac{\partial vu}{\partial y}+\frac{\partial wu}{\partial z}=fv-\frac{1}{\rho_0}\frac{\partial q}{\partial x}-g\frac{\partial \eta}{\partial x}-\frac{1}{\rho_0}\frac{\partial p_a}{\partial x}-\frac{g}{\rho_0}\int_z^\eta \frac{\partial \rho}{\partial x}dz+F_u+\frac{\partial}{\partial z}\left(\nu_t^v\frac{\partial u}{\partial z}\right) \quad \text{(A1.2.1)}$$

609

610 $$\frac{\partial v}{\partial t}+\frac{\partial v^2}{\partial y}+\frac{\partial uv}{\partial x}+\frac{\partial wv}{\partial z}=fu-\frac{1}{\rho_0}\frac{\partial q}{\partial y}-g\frac{\partial \eta}{\partial y}-\frac{1}{\rho_0}\frac{\partial p_a}{\partial y}-\frac{g}{\rho_0}\int_z^\eta \frac{\partial \rho}{\partial y}dz+F_v+\frac{\partial}{\partial z}\left(\nu_t^v\frac{\partial v}{\partial z}\right) \quad \text{(A1.2.2)}$$

611

612 $$\frac{\partial w}{\partial t}+\frac{\partial w^2}{\partial z}+\frac{\partial uw}{\partial x}+\frac{\partial wv}{\partial y}=-\frac{1}{\rho_0}\frac{\partial q}{\partial z}+F_w+\frac{\partial}{\partial z}\left(\nu_t^v\frac{\partial w}{\partial z}\right) \quad \text{(A1.2.3)}$$

613

614 $$\frac{\partial T}{\partial t}+\frac{\partial uT}{\partial x}+\frac{\partial vT}{\partial y}+\frac{\partial wT}{\partial z}=F_T+\frac{\partial}{\partial z}\left(D_{ts}^v\frac{\partial T}{\partial z}\right)+\hat{H} \quad \text{(A1.3)}$$

615

616 $$\frac{\partial S}{\partial t}+\frac{\partial uS}{\partial x}+\frac{\partial vS}{\partial y}+\frac{\partial wS}{\partial z}=F_s+\frac{\partial}{\partial z}\left(D_{ts}^v\frac{\partial S}{\partial z}\right) \quad \text{(A1.4)}$$

617

618 $$\rho=\rho(S,T) \quad \text{(A1.5)}$$

619 Since we used the barotropic density mode the only hydrodynamic equations used for the present work
620 are A1.1 and A1.2. The symbols used in the governing equations of the model are presented in Table 4

https://doi.org/10.5194/os-2020-90
Preprint. Discussion started: 17 September 2020

621 **Table 4 – Symbols used in the governing equations A1**

x,y,z	Cartesian coordinate system
u,v,w	components of the field of velocity [ms^{-1}]
g	gravity acceleration [ms^{-2}]
ρ	water density [kgm^{-3}]
ρ_0	reference value for water density [kgm^{-3}]
q	non-hydrostatic pressure [Pa]
p_a	atmospheric pressure at the sea surface [Pa]
f	Coriolis parameter (non dimensional)
v_t^v	vertical eddy viscosity [m^{2}s^{-1}]
F_u, F_v, F_w	horizontal diffusivity
T	temperature [°C]
S	Salinity [PSU]
F_T, F_S	Horizontal diffusion terms for T and S
D_{ts}^v	vertical eddy diffusivity [m^{2}s^{-1}]
$\hat{H}$	Source term due to heat exchange with the atmosphere

622

623 **APPENDIX A2 – Mud transport model governing equations and parameterizations**

624 The sediment transport module is based on the advection dispersion equation for a passive tracer in an incompressible
625 fluid. The tracer is the concentration C of sediment along the water column. The field velocity used for advection is the
626 one calculated through the hydrodynamic set of equations of Appendix A1. The symbols used in the set of equations A2
627 are summarized in Table 5

628 $$\frac{\partial C}{\partial t} + \frac{\partial}{\partial x}(uC) + + \frac{\partial}{\partial y}(vC) + \frac{\partial}{\partial z}[(w + w_s)C] = \frac{\partial}{\partial z}\left(D_C^v \frac{\partial C}{\partial z}\right) + F_C \quad \text{(A2.1)}$$

629 The vertical bottom boundary condition for sediment flux is expressed as:

630 $$D_C^v \frac{\partial C}{\partial z}\Big|_{z=-H} - w_s C = S \quad \text{(A2.2)}$$

631 and the sediment flux S at the bottom is calculated through the approach of Krone (Krone, 1962) for deposition (Eq.
632 A2.3), through that of Partheniades (Partheniades, 1965) for erosion of consolidated sediment (Eq. A2.4) and through
633 that of Parchure and Metha (Parchure and Metha, 1985) for erosion of soft or unconsolidated sediment (Eq. A2.5).

634 $$S_d = w_s c_b p_d \quad \text{(A2.3)}$$

635 where

636 $$p_d = 1 - \frac{\tau_b}{\tau_{cd}} \qquad \text{valid for } \tau_b < \tau_{cd} \quad \text{(A2.3.1)}$$

637 $$S_{ec} = E\left(\frac{\tau_b}{\tau_{ce}} - 1\right)^n \qquad \text{valid for } \tau_b \geq \tau_{ce} \text{ and hard bed} \quad \text{(A2.4)}$$

https://doi.org/10.5194/os-2020-90
Preprint. Discussion started: 17 September 2020

638 $$S_{es} = E\ exp\left[\alpha(\tau_b - \tau_{ce})^{1/2}\right] \qquad \text{valid for } \tau_b \geq \tau_{ce} \text{ and soft bed} \qquad \text{(A2.5)}$$

639 The settling velocity for sediment is calculated through the Stokes law (A2.6).

640 $$w_s = \frac{gd^2}{18}\left(\frac{\rho_s}{\rho_w} - 1\right) \qquad \text{(A2.5)}$$

641 **Table 5 – symbols used in the equations and parameterizations A2 of the sediment transport model**

x,y,z	cartesian coordinate system (same as Table 4)
u,v,w	components of the field of velocity (same as Table 4) [ms^{-1}]
C	sediment concentration [gmc^{-1}]
C_b	sediment concentration in the bottom layer [gmc^{-1}]
w_s	settling velocity [ms^{-1}]
D_C^v	vertical eddy diffusivity for C (same as for T and S) [m^2s^{-1}]
F_C	horizontal diffusion terms for C
H	water depth [m]
S_e	bottom sediment flux for erosion [kgm^2s^{-1}]
S_d	bottom sediment flux for deposition [kgm^2s^{-1}]
$S_{e,s}$	bottom sediment flux for erosion of soft bed [kgm^2s^{-1}]
$S_{e,c}$	bottom sediment flux for erosion of consolidated bed [kgm^2s^{-1}]
p_d	probability of deposition for the sediment [non dimensional]
τ_b	bottom shear stress [Nm^{-2}]
τ_{bd}	critical stress for deposition [Nm^{-2}]
τ_{ce}	critical stress for erosion [Nm^{-2}]
E	bottom erodibility [Nm^{-2}]
α	empirical coefficient [$m/\sqrt{N}$]
n	Power of erosion (empirical non-dimensional)
d	diameter of grains [m]
ρ_s	density of dried sediment [kgm^{-3}]
ρ_w	density of water[kgm^{-3}]
g	gravity acceleration [ms^{-2}]

642

643 **Data Availability**

644 The modelling dataset including the simulations produced for the present study covers a volume wider than 2 TB. Such
645 an amount of data raises an evident problem in order to make them available on data repositories. Consequently, the
646 output of the simulations won't be directly available. However, the model set-up and all the files necessary for their
647 reproduction will be made available in MIKE FM format upon request to the corresponding author.

648

649 **Team list**

650 Antonio Guarnieri (first and corresponding author), Sina Saremi (co-author), Andrea Pedroncini (co-author), Jakob H.
651 Jensen (co-author), Silvia Torretta (co-author), Caterina Vincenzi (co-author), Marco Vaccari (co-author).

652

653 **Author contributions:**

https://doi.org/10.5194/os-2020-90
Preprint. Discussion started: 17 September 2020

Antonio Guarnieri implemented the numerical models and simulations, post-processed the raw output, analysed the results and wrote the manuscript;

Sina Saremi gave technical and scientific support during the implementation of the models, provided the code for the propellers modelization as input to MIKE and supported the writing and finalization of the manuscript;

Andrea Pedroncini first conceived the idea of the methodology adopted in the study, gave scientific support for the implementation of the models and feedback during the writing of the manuscript;

Jacob H. Jensen provided scientific support and advice regarding the driving mechanisms of naval induced sediment dynamics;

Silvia Torretta provided technical support for the model implementation and for the observed bathymetry analysis and reconstruction;

Caterina Vincenzi and Marco Vaccari provided bathymetry data, sediment data and information on dredging activities and general sediment related issues. They also favored the acquisition of the naval traffic data.

Competing interests:

Caterina Vincenzi and Marco Vaccari are employees of the Port Authority of Genova (Autorità di Sistema Portuale del Mar Ligure Occidentale), which commissioned and funded the present study to DHI, a private not-for-profit consultancy and research company in the field of water. Andrea Pedroncini, Silvia Torretta, Sina Saremi and Jakob H. Jensen are DHI employees. Antonio Guarnieri was DHI employee when the study was conducted; he is now employed at Istituto Nazionale di Geofisica e Vulcanologua (INGV).

Acknowledgments

We are grateful to Stazioni Marittime SpA for providing the daily traffic data of the Port of Genoa which was the starting point for this study. We are particularly grateful to Captain Calcagno of Stazioni Marittime SpA for the qualified and experienced information he gave on the sediment and vessels' dynamics in the port, which helped set up the numerical models, interpret and rely on the final results.

References

- Abromeit, U., Alberts, D., Fischer, U., Fleischer, P., Fuehrer, M., Heibaum, M., Kayser, J., Knappe, G., Köhler, H.J., Liebrecht, A., Reiner, W., Schmidt-vöcks, D., schulz, H., Schuppener, B., Söhngen, B., Soyeaux, R.: Principles for the Design of Bank and Bottom Protection for Inland Waterways, 1st Edition, Bundesanstalt für Wasserbau, Karlsruhe, 2010.

https://doi.org/10.5194/os-2020-90
Preprint. Discussion started: 17 September 2020

685 • Castells, M. , Mujal-Colilles, A., Llull, T., Gironella, X., Martínez de Osés, V., Martín A., and Sánchez-
686 Arcilla, A.: Ship manoeuvre patterns to prevent propeller scouring effects, 34th PIANC-World Congress,
687 Panama, 7-11-May 2018, A-238, 2018.
688 • Ciccacci, S., D'Alessandro, L., Fredi, P., and Lupia Palmieri, E. (1989). Contributo dell'analisi geomorfica
689 quantitativa allo studio dei processi di denudazione nel bacino idrografico del Torrente Paglia (Toscana
690 meridionale - Lazio settentrionale),Suppl. Geogr. Phys. Dinam. Quat., I, 171-188,
691 https://doi.org/10.13140/2.1.2991.6802, 1989.
692 • CIRIA, CUR, CETMEF: The Rock Manual. The use of rock in hydraulic engineering, 2nd edition, C683
693 CIRIA, London, 2007.
694 • DHI: MIKE 3 Flow Model HD FM - Hydrodynamics Flexible Mesh - Scientific Documentation, DHI,
695 Hørsholm, 2017.
696 • DHI: MIKE 3 MT FM - Mud Transport Flexible Mesh - Scientific Documentation, DHI, Hørsholm, 2019.
697 • Flather, R.: A tidal model of the northwest European continental shelf, Memories de la Societe Royale des
698 Sciences de Liege, 6, 10, 141–164, 1976.
699 • Grabe, J., Van Audgaerden, T., Busjaeger, D., Gerrit de Gijt, J., Heibaum, M., Heimann, S., Van der Horst, A.,
700 Kalle, H.U, Krengel, R., Lamberts, K.H., Miller, C., Morgen, K., Peshken, G., Retzlaff, T., Reuter, E.,
701 Richwein, W., Ruland, P., Schrobenhausen, W. S., Tworushka, H., Vollstedt, H.W.: Recommendations of the
702 Committee for Waterfront Structures, Harbours and Waterways - EAU 2012, 9th Edition, Issued by the
703 Committee of Waterfront Structures of the German Port Technology Association and the German Geotechnical
704 Society, Ernst & Sohn GmbH & Co., Berlin, 661, 2015.
705 • Grant W. and Madsen O.: Combined wave and current interaction with a rough bottom, J. Geophys. Res., 84,
706 1797–1808, 1979.
707 • Hamill, G.A.: Characteristics of the screw wash of a manoeuvring ship and the resulting bed scour, Ph.D.
708 dissertation, Queen's Univ. of Belfast, Belfast, Northern Ireland, 1987.
709 • Hong, J. H., Chiew, Y.M, Hsieh, S. C., Cheng, N.S., and Yeh, P.H.: Propeller Jet–Induced Suspended-
710 Sediment Concentration, J. of Hydraul. Eng., 142, 2, https://doi.org/10.1061/(ASCE)HY.1943-7900.0001103,
711 2016.
712 • Kristensen, H. O.: Analysis of technical data of Ro-Ro ships, in: Report n. 02 - of Project n. 2014-122
713 Mitigating and reversing the side-effects of environmental legislation on Ro-Ro shipping in Northern Europe,
714 HOK Marineconsult ApS, 2016.

https://doi.org/10.5194/os-2020-90
Preprint. Discussion started: 17 September 2020

- Krone, R.: Flume studies of the transport of sediment in estuarial processes: Final Report, Hydraulic Engineering Laboratory and Sanitary Engineering Research Laboratory, Univ. of California, Berkely, 1962.
- Lam, W., Hamill, G., Robinson, D., Raghunathan, R., and Kee, C., Submerged propeller jet, WSEAS Conferences, Udine, Italy, 20-22 January 2005.
- Leonard, B.P.: The ULTIMATE conservative difference scheme applied to unsteady one-dimensional advection, Comput. Method Appl. M., 88, 17-74, https://doi.org/10.1016/0045-7825(91)90232-U, 1991.
- Lisi, I., Feola, A. , Bruschi, A., Di Risio, M., Pedroncini, A., Pasquali, D., and Romano, E.,: La modellistica matematica nella valutazione degli aspetti fisici legati alla movimentazione dei sedimenti in aree marino-costiere, Manuali e Linee Guida ISPRA, 169/2017, 144., 2017.
- MarCom Working Group 180: PIANC REPORT N° 180 - Guidelines for Protecting Berthing Structures from Scour Caused by Ships, PIANC Secrétariat Général., Bruxelles, 2015.
- Mujal-Colilles, A., Gironella, X., Sanchez-Arcilla, A., Puig Polo, C., and Garcia-Leon, M.: Erosion caused by propeller jets in a low energy harbour basin, J. Hydraul. Eng., https://doi.org/10.1080/00221686.2016.1252801, 2016.
- Parchure, T., and Metha, A.: Erosion of soft cohesive sediment deposits, J. of Hydraul. Eng., 111, 10, 1308-1326, https://doi.org/10.1061/(ASCE)0733-9429(1985)111:10(1308), 1985.
- Partheniades, E.: Erosion and deposition of cohesive soils, Journal of the Hydraulics Division, 91, 105-139, 1965.
- Rapaglia, J., Zaggia, L., Ricklefs, K. , Gelinas M., and Bokuniewicz, H.: Characteristics of ships' depression waves and associated sediment resuspension in Venice Lagoon, Italy: J. Marine Syst., 85, 45-56, https://doi.org/10.1016/j.jmarsys.2010.11.005, 2011.
- Soulsby, R., Hamm, L. , Klopman, G., Myrhaug, D., Simons, R., and Thomas, G.: Wave-current interaction within and outside the bottom boundary layer, Coast. Eng., 21, 41-69, 1993.
- Teeter, A.: Vertical transport in fine-grained suspension and nearly-deposited sediment, in: Estuarine Cohesive Sediment Dynamics, 14, Mehta, A.J., Springer Verlag, 126-149, https://doi.org/DOI:10.1029/LN014, 1986.
- UNESCO, The practical salinity scale 1978 and the international equation of state of sea water, UNESCO Technical Papers in Marine Science 36, 25 pp.,1981a."
- Van Rijn, L.: Unified view of sediment transport by currents and waves. Initiation of motion, bed roughness, and bed-load transport, J. Hydraul. Eng., 133, 6, 2007.

https://doi.org/10.5194/os-2020-90
Preprint. Discussion started: 17 September 2020

744 • Verhei, H. J.: The stability of bottom and banks subjected to the velocities in the propeller jet behind ships, 8th
745 International Harbour Congress, Antwerp, June 13-17, 303, 1983.
746 • Winterwerp, J., and Van Kesteren, W.: Introduction to the Physics of Cohesive Sediment in the Marine
747 Environment, 1st Edition, 56, Elsevier B.V., Amsterdam, 576, 2004.